applied sciences

Article

Terahertz Emission Enhanced by a Laser Irradiating on a T-Type Target

Ji Zhang [1], Xiaona Ban [1], Feng Wan [2,*] and Chong Lv [1,*]

[1] Department of Nuclear Physics, China Institute of Atomic Energy, Beijing 102413, China; zhangji401@sina.com (J.Z.); banxiaona@ciae.ac.cn (X.B.)
[2] Ministry of Education Key Laboratory for Nonequilibrium Synthesis and Modulation of Condensed Matter, School of Physics, Xi'an Jiaotong University, Xi'an 710049, China
* Correspondence: wanfeng@xjtu.edu.cn (F.W.); lvchong@ciae.ac.cn (C.L.)

Abstract: The generation of high field terahertz emission based on the interaction between an ultra-intense laser and solid targets has been widely studied in recent years because of its wide potential applications in biological imaging and material science. Here, a novel scheme is proposed to enhance the terahertz emission, in which a linearly polarized laser pulse irradiates a T-type target including a longitudinal target followed by a transverse target. By using two-dimensional particle-in-cell simulations, we find that the electron beam, modulated by the direct laser acceleration via the interaction of the laser with the longitudinal solid target, plays a crucial role in enhancing the intensity of terahertz emission and controlling its spatial distribution. Compared with the single-layer target, the maximum radiated electromagnetic field's intensity passing through the spatial probe point is enhanced by about one order of magnitude, corresponding to the terahertz emission power increasing by two orders of magnitude or so. In addition, the proposed scheme is robust with respect to the thickness and length of the target. Such a scheme may provide important theoretical and data support for the enhancement of terahertz emission efficiency based on the ultra-intense laser irradiation of solid targets.

Keywords: terahertz emission; T-type target; laser–plasma interaction; PIC simulation; electron acceleration

Citation: Zhang, J.; Ban, X.; Wan, F.; Lv, C. Terahertz Emission Enhanced by a Laser Irradiating on a T-Type Target. *Appl. Sci.* **2022**, *12*, 4464. https://doi.org/10.3390/app12094464

Academic Editor: Saulius Juodkazis

Received: 23 March 2022
Accepted: 25 April 2022
Published: 28 April 2022

1. Introduction

The terahertz (THz) wave is in a special frequency band in the transition from electronics to photonics and has the characteristics of low radiation dose, good transmittance, etc. Therefore, THz radiation sources are widely used in frontier basic science fields, such as nonlinear THz optics [1], condensed matter physics, material science [2,3], and life science research [4–6], as well as their important applications in non-destructive testing [7], THz wave radar detection, [8] and other technical fields. Among the THz wave generation methods, there are THz emission sources driven based on the electrons accelerated by conventional accelerators [9] and THz wave radiation sources driven by optical rectification [10–12] and photoconductive antennas [13]. In addition, with the rapid development of laser–plasma interaction physics, the generation of THz emission based on laser–plasma has been extensively studied, because the plasma itself does not have a breakdown threshold. For example, Cook et al. proposed a scheme of using a two-color laser with 800 nm fundamental frequency and 400 nm doubled frequency light to ionize air into filaments to enhance the generation of THz emission [14]. The energy conversion efficiency in the experiments was three orders of magnitude higher than that of 800 nm fundamental frequency light. Subsequently, many researchers have proposed a series of schemes to enhance or modulate THz emission, such as changing the frequency ratio of the two-color laser [15], filling different types of gases in the vacuum tube [16], using a three-color laser field [17], applying an external axial magnetic field [18] and optimization parameters, and so on.

However, the laser defocusing caused by plasma and the absorption by the air make the generated THz emission appear saturated, resulting in the intensity and energy of the THz emission no longer increasing with the increase in the laser intensity.

Recent studies have shown that based on the ultra-intense laser irradiating on solid targets, THz emission with higher intensities and more energies can be obtained [19–21]. For instance, Ding et al. [22] simulated that the half-cycle THz wave, based on the coherent transition radiation (CTR) mechanism [23,24], could be radiated by the forward (or backward) fast electrons passing through the front (or rear) target–vacuum interfaces when a laser interacted with a solid foil. Subsequently, a large number of experiments have been carried out to study the generation of THz emission by the femtosecond (fs) or picosecond (ps) laser irradiating a solid target [25–27], and the obtained energy has reached $\sim$50 mJ [26]. Meanwhile, Liao et al. [28] have also experimentally and theoretically investigated how to manipulate the THz spectrum by varying the laser pulse duration or target size when the ultra-intense laser pulse interacts with a foil target. In addition, in order to regulate or improve the efficiency of THz emission, researchers have carried out a large number of theoretical or experimental studies based on the interaction of lasers and structural targets to generate THz emission. For example, high energy and well-collimated electron bunches, produced and accelerated by the microplasma waveguide (MPW), can be converted to strong THz emission via coherent diffraction radiation (CDR) [29] when exiting the MPW, corresponding to efficiency exceeding 1% [30]. Apart from the MPW, the scheme of laser-irradiated wires, microtapes, or a surface of a solid target, has been widely applied in the theoretical, simulation, and experimental studies of laser plasma physics, such as the electron acceleration by the longitudinal field of a surface plasma wave (SPW) [31–34], dense electron generation and acceleration by a wire [35–40], protons acceleration [41–44], γ-ray and electron-positron pair generation [45,46], and so on. Furthermore, the laser-irradiated wires have efficiently generated THz emission due to fast electrons undergoing helical motion [47–50] or a current-carrying line antenna [51]. However, it is currently unclear how a flat thin target placed longitudinally affects the THz emission via the CTR.

In this paper, a T-type target (TTT) including a longitudinal target and a transverse target is proposed and investigated by using two-dimensional (2D) particle-in-cell (PIC) simulations. The result shows that the TTT can significantly enhance the intensity of THz emission and affect its spatial distribution. Compared with the case of single-layer target (SLT), the maximum intensity of the THz emission passing through the spatial probe point in the (x, y) plane is enhanced by more than one order of magnitude, and the THz emission along the rear surface exhibits a much weaker distribution in the center than that at both wings. We analyze the interaction processes of the laser, respectively, with the longitudinal target and transverse target in detail through a series of simulations and clarify the origin of high energy electrons. In addition, the robustness of this scheme is also verified by the target parameters scanning.

The paper is organized as follows. Section 2 outlines the target configurations and laser and plasma parameters. Section 3 shows the simulation results. In addition, the reasons why THz emission was enhanced by a laser irradiating on a TTT are also discussed in detail in Section 4. Furthermore, Section 5 presents a robust analysis. Lastly, a brief summary is given in Section 6.

2. Simulation Setup

In order to demonstrate the enhancement effect of the TTT on THz emission and the physical reasons for it, we used the PIC code of open source EPOCH [52] and carried out a series of 2D simulations. For the TTT scheme, the initial setup in the simulations is displayed in Figure 1. The simulation box was located at the (x, y) plane, and the simulation region was set as $200\lambda_0 \times 100\lambda_0$ with 6000×2000 grids, where $\lambda_0 = 1.0$ μm was the laser's wavelength. In addition, the quasi-particle number of every cell was 50 per kind of particle. Both targets I and II were composed of a material (we assume gold, Au) and electrons were utilized as the TTT. The TTT-I was distributed from $5\lambda_0 \le x \le 75\lambda_0$ along the x-axis and $-2\lambda_0 \le y \le 2\lambda_0$ along the y-axis, with number density $n_{e0} = 50n_c$, while the TTT-II was distributed from $75\lambda_0 \le x \le 80\lambda_0$ with $n_{e0} = 50n_c$, where $n_c = m_e\omega_0^2/4\pi e^2$ was the critical plasma number density, with m_e being the electron mass, e being the electron charge, and ω_0 being the laser frequency. Since the laser intensity was much larger than the ionization potential of the Au ions [44,53,54], they were assumed to be ionized to Au^{50+} due to the limitation of the computing resources. Furthermore, the ions were mobile in all of the simulations. As a comparison, the SLT located at $75\lambda_0 \le x \le 80\lambda_0$ with only target II $n_{e0} = 50n_c$ was set in the simulations. Meanwhile, it should be noted that we also performed a series of simulations on other material (CH), and the obtained results were qualitatively consistent with the case of Au. Moreover, it is appropriate not to include collisions since the collisional absorption is dominant at a much lower intensity [55–58].

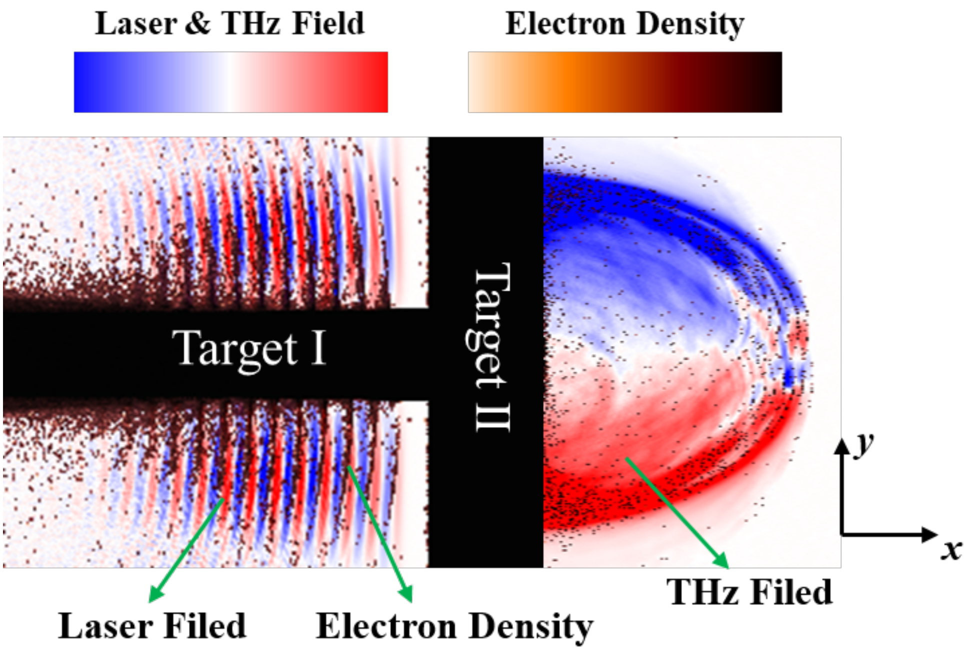

Figure 1. The features of the T-type target structure and the terahertz waves radiated behind the target by the coherent transition radiation (CTR) mechanism. Target I refers to the longitudinal target, while Target II stands for the transverse target. The electrons in Target I are pulled out and accelerated to very high energy, and they radiate terahertz waves after passing through Target II.

A transverse Gaussian and p-polarized laser with temporal and spatial profile $I = I_0 \exp[-(t-t_0)^2/\tau_0^2]\exp(-y^2/r_0^2)$ was normally incident from the left boundary of the simulation box. The peak intensity was $I_0 = 6.0 \times 10^{20}$ W/cm^2, corresponding to the normalized vector potential $a_0 = eE_0/m_e c\omega_0 = 21$ for $\lambda_0 = 1.0$ µm. Furthermore, the laser parameters $r_0 = 6.0\lambda_0$ and $t_0 = \tau_0 = 5T_0$ were set to fixed values in all simulations, where T_0 was the laser period. In addition, the x-direction and y-direction were the absorption boundary for both fields and particles, respectively.

3. Results

Now, let us demonstrate the effect of THz emission enhancement in TTT. Firstly, the spatial distributions of the radiated electromagnetic fields (including the electric field E_y + magnetic field B_z) are shown in Figure 2 for both cases of SLT and DLT at different times $t = 90T_0$ and $t = 120T_0$. We could note that they were radiated by the forward fast electrons passing through the rear target–vacuum interfaces. Yet, the radiated electromagnetic field can be significantly enhanced under the action of TTT. Furthermore, from Figure 2b,d, the intensity of the radiated electromagnetic field was an order of magnitude higher in the case of TTT than that in the case of SLT. In addition, on the one hand, unlike that of the

SLT, when the THz emission was just generated behind the target, it produced two sets of radiation field distributions, as shown in Figure 2c. This indicates that they originated from two different electron sources. On the other hand, for the generated THz emission through the CTR in SLT, it emitted from the point sources around the laser irradiation spot at the rear side, and the strongest emission was along the target surfaces [22], as shown in Figure 2b. However, in TTT from Figure 2d, the radiated electromagnetic field along the rear surface exhibited a much weaker distribution in the center than at both wings, rather than traveling around the laser irradiation spot behind the target.

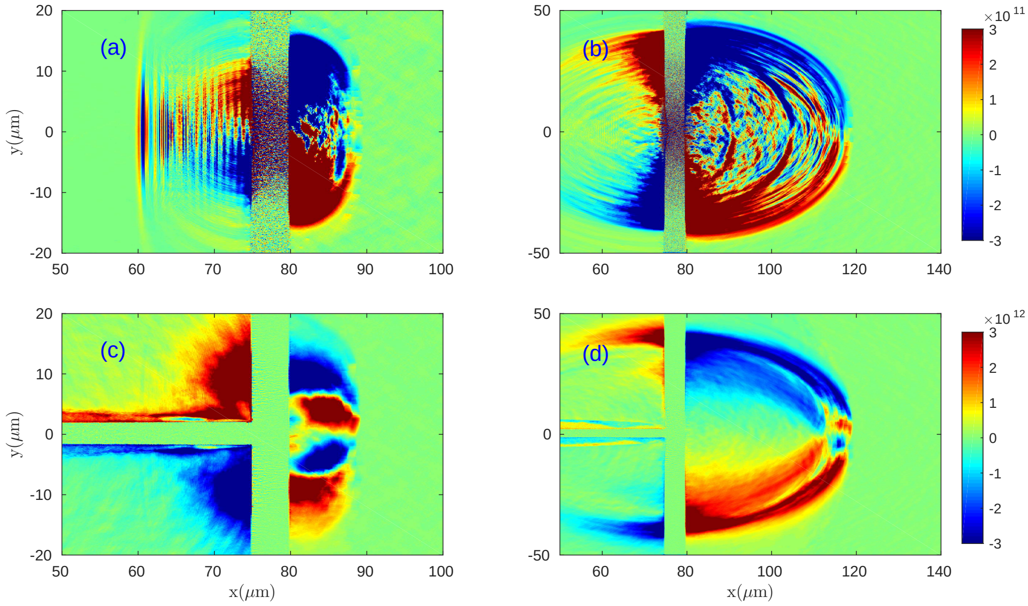

Figure 2. Two−dimensional spatial distributions of the radiated electromagnetic field in the case of SLT (**a**,**b**) and in the case of TTT (**c**,**d**) at different times $t = 90T_0$ and $t = 120T_0$.

In order to further quantitatively demonstrate the enhancement effect of the TTT on THz emission and whether it was in the THz band, both time-domain and frequency-domain spectra of the radiated electromagnetic field passing through the space point $(146.67\lambda_0, -20.0\lambda_0)$ at the (x, y) plane for the SLT and TTT were, respectively, given, as shown in Figure 3. On the one hand, from the time-domain spectra of the radiated electromagnetic field in Figure 3a, the black line showed that the maximum in the case of the SLT was about 0.3 TV/m. However, the maximum value in the case of the TTT reached about 2.8 TV/m, which was greatly enhanced by an order of magnitude or so. On the other hand, from the frequency-domain spectra of the radiated electromagnetic field in Figure 3b, it showed that the generated THz emission was in the THz band. Furthermore, the maximum frequency of the generated THz wave reached 150 THz, which also proved that the THz wave generated by the interaction between the laser and plasma had the characteristics of wide bandwidth. Additionally, after integrating the spectrum curve, we also see that the power of the THz emission generated in the TTT was enhanced by about two orders of magnitude compared to that in the SLT. Therefore, the above results quantitatively prove that the TTT can significantly enhance the generation of THz emission.

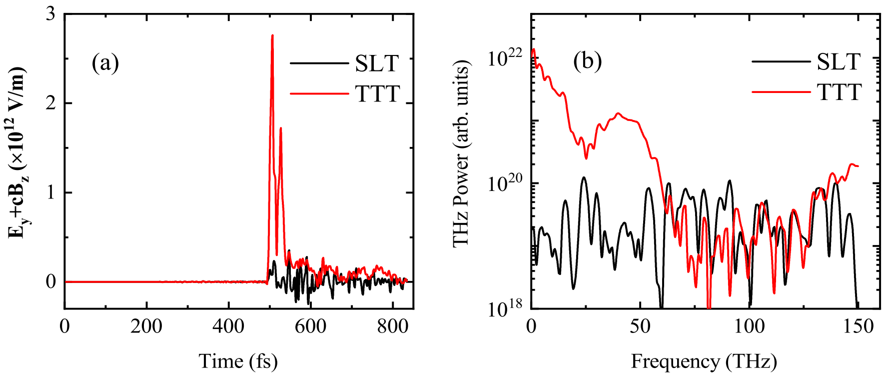

Figure 3. The radiated electromagnetic field passing through the space point (146.67λ_0, −20.0λ_0) at the (x, y) plane for the SLT and TTT. (**a**) The time-domain waveforms of the radiated electromagnetic field; (**b**) The frequency-domain spectra in logarithmic scale.

4. Discussion

Section 3 demonstrated that the TTT can enhance THz emission generation. Since the principle of generating THz emission was mainly dominated by the CTR in this work, the parameters, such as the number density, distribution, and energy of fast electrons behind the target, were the origin of the generation of THz emission.

Figure 4 shows the two-dimensional spatial number density distribution of fast electrons for both the SLT and TTT at different times, $t = 90T_0$ and $t = 120T_0$, respectively. To clarify the physical mechanism by which the TTT enhanced THz emission, we used some settings in the EPOCH codes to distinguish the fast electrons from Target I and Target II. Among them, Figure 4c,d shows the number density distribution of fast electrons in Target II at different time, while Figure 4e,f shows those in Target I. First, we can observe that almost no electrons moved behind the target in Target II, either earlier or later. This means that the electrons in Target II did not gain much energy from the laser, and the corresponding contribution to the THz emission generation was almost non-existent. In addition, we can also observe that the electrons in Target II moved along the negative direction of the x-axis in Target I, which was due to the forward movement of electrons in Target I leading to the electrons' return current in Target II. On the contrary, a large number of electrons were pulled out from Target I and moved to the backside of the target, which means that the fast electrons that enhanced the THz emission originated from Target I. At the same time, it is also noticed that the fast electrons appeared in two regions behind the target at an earlier moment from Figure 4e: (i) the fast electrons with lower energy were located around the laser irradiation spot at the rear side; (ii) the electrons with higher energy were distributed symmetrically in the two wing regions. The above fast electrons' density distribution led to the appearance of two sets of THz emission, as shown in Figure 2c. Over time, most high-energy electrons appeared to be distributed at both wings of the target backside, causing the intensities of THz emission to be higher on the wings than that of the central region, which is, respectively, shown in Figures 4f and 2d. Yet, the fast electrons from both forward and backward of the SLT had a transverse Gaussian profile in the central region similar to the shape of the laser, as shown in Figure 4a,b, which explains why the generated THz emission radiates to the surroundings with this point as the source center.

In addition to the modulation of the spatial profile of the THz emission by the fast electrons' number density distribution, the energy of the fast electrons can have a significant effect on the intensity of the THz emission. Figure 5 shows the energy spectrum distribution of the fast electrons for both the SLT and TTT at different times, $t = 90T_0$ and $t = 120T_0$. Compared with the case of SLT, the fast electron energy generated in the case of TTT was significantly higher: the maximum cutoff energy of the fast electrons generated in TTT was about 140 MeV, while that in SLT was only about 20 MeV. The fast electrons of such high energy in TTT naturally radiate higher THz wave intensity through the CTR when they pass through the vacuum interface behind the target. Meanwhile, we can also observe from Figure 2a,c, that a part of the laser pulse was obviously not absorbed but reflected at the range 60 µm < x < 70 µm in the case of SLT, while it did not appear in the case of TTT. From this point of view, it also shows that the TTT can significantly enhance the energy coupling between the laser and plasma. In addition, by comparing the blue curve with the black curve in Figure 5a,b, the maximum cutoff energy of the fast electrons in TTT-II was dramatically smaller than that in SLT, which also quantitatively indicates that the fast electrons enhancing the THz emission were mainly derived from TTT-I.

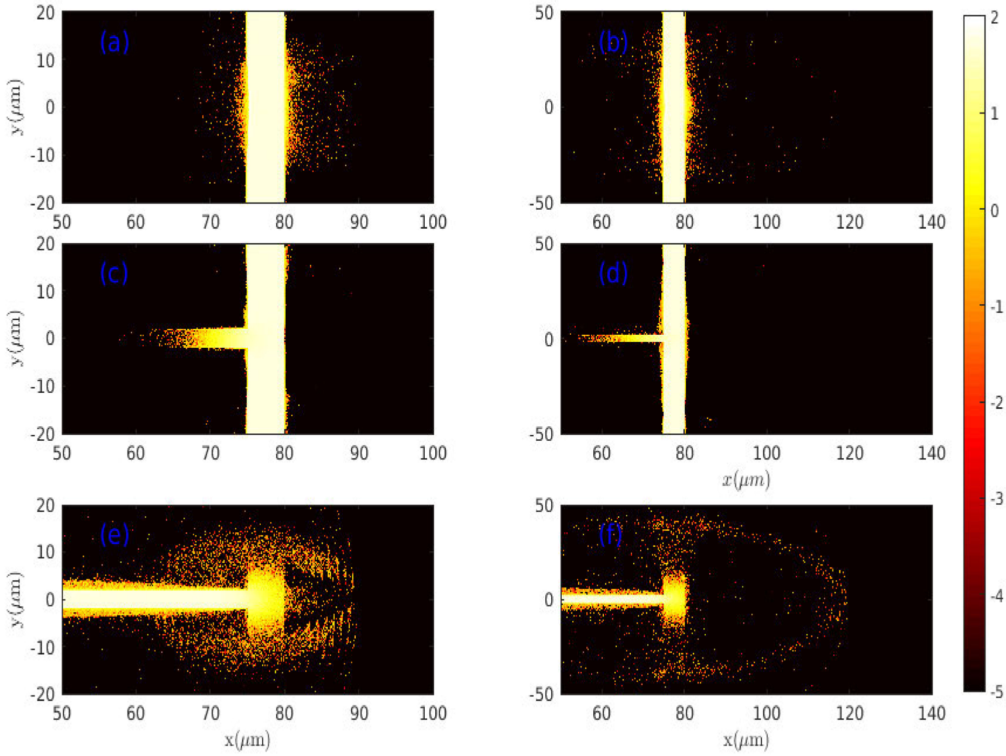

Figure 4. Two−dimensional spatial distributions in a logarithmic of the electron number density in the case of SLT (**a**,**b**), in the case of TTT-II (**c**,**d**), and in the case of TTT-I (**e**,**f**) at different times, $t = 90T_0$ and $t = 120T_0$. The electron number density is normalized by the electron plasma critical density n_c.

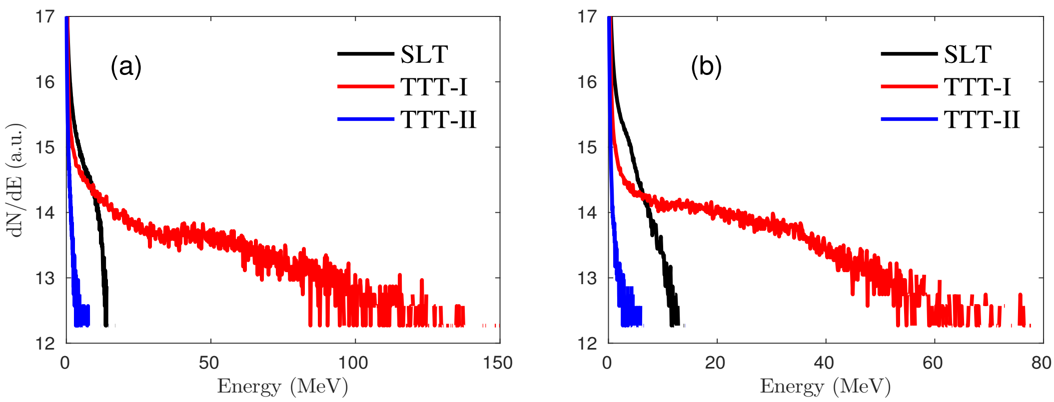

Figure 5. The electron energy in the case of SLT and TTT at different times, $t = 90T_0$ (**a**) and $t = 120T_0$ (**b**). The black curve, blue curve, and red curve represent the electron spectrum distributions of SLT, TTT-II, and TTT-I, respectively. The statistics of the electron energy distribution count the energy of all electrons in the simulation area.

We carried out a detailed analysis of the mechanism of generating high-energy electrons. Similar to the direct laser acceleration, the SPW could only be excited in the case of

p-polarized lasers [59]. To clarify which acceleration mechanism dominated, we state that the energy gain was only due to the electric field and could be divided into a longitudinal (dominated by the SPW) and a transverse component (dominated by the direct laser acceleration). We integrated over time from 0 to t to obtain the gain components for each numerical electron [44,60],

$$\Gamma_x = -\int_0^t ev_x E_x dt, \tag{1}$$

$$\Gamma_y = -\int_0^t ev_y E_y dt. \tag{2}$$

The electron distribution in the energy gain space of (W_x, W_y) is shown in Figure 6. The black dashed line corresponds to the $W_x + W_y = 0$, while the red dashed line ($W_x = W_y$) divides the space into two regions: direct laser acceleration-dominated region in the upper left and the SPW-dominated region in the lower right, respectively. One could note that more electrons gained more energy from the transverse field of the direct laser acceleration than that from the longitudinal field of SPW. So this proves that the higher energy electrons came from the contribution of the direct laser acceleration.

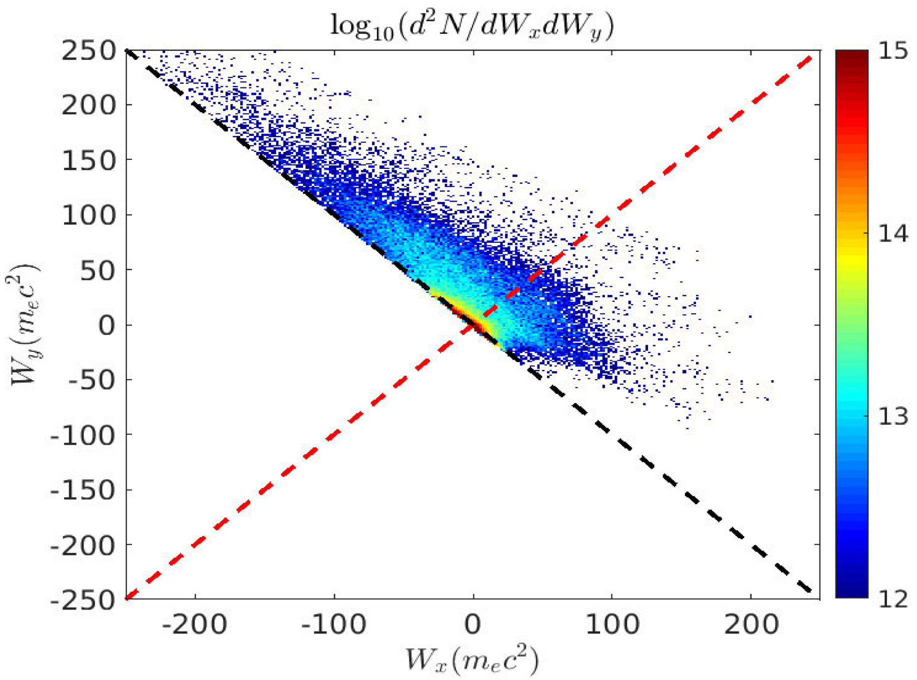

Figure 6. The energy gain from the longitudinal (large W_x) and transverse (large W_y) acceleration. The red dashed line represents the $W_x = W_y$, and the black dashed line represents the $W_x + W_y = 0$.

5. Robustness of the Scheme

Taking into account the effects of the laser and target parameters in the realistic experiments, we performed a series of PIC simulations to investigate the robustness of our scheme. We scanned the effect of THz emission intensity by varying parameters such as the length and thickness of Target I in our simulations. It should be noted that in order to be able to compare effectively, the position of the detection point was unchanged relative to the position of Target II. The results are plotted in Figure 7. We found that although the parameters could slightly affect the maximum intensity of the radiated electromagnetic field, without exception, they were greatly improved compared to the case of SLT. We also plotted the relationship between the power of the THz emission and the length and thickness of Target-I, as shown in Figure 7b,d. We found that the THz emission was affected when changing the parameters, either the length or the thickness of Target-I. It can be concluded: (i) As the length of Target-I increased, the power of the THz emission increased gradually and tended to saturate slowly. This is because as the length increased, more electrons were produced. (ii) As the thickness of Target-I decreased, the power of THz emission also increased gradually. This is mainly because as the thickness decreased, it was closer to the center of the laser focal spot, when the laser interacted with the target surface. However, the thickness should not be too small, otherwise, the laser will ablate and destroy the Target-I. All of the above results demonstrate that this scheme is very robust.

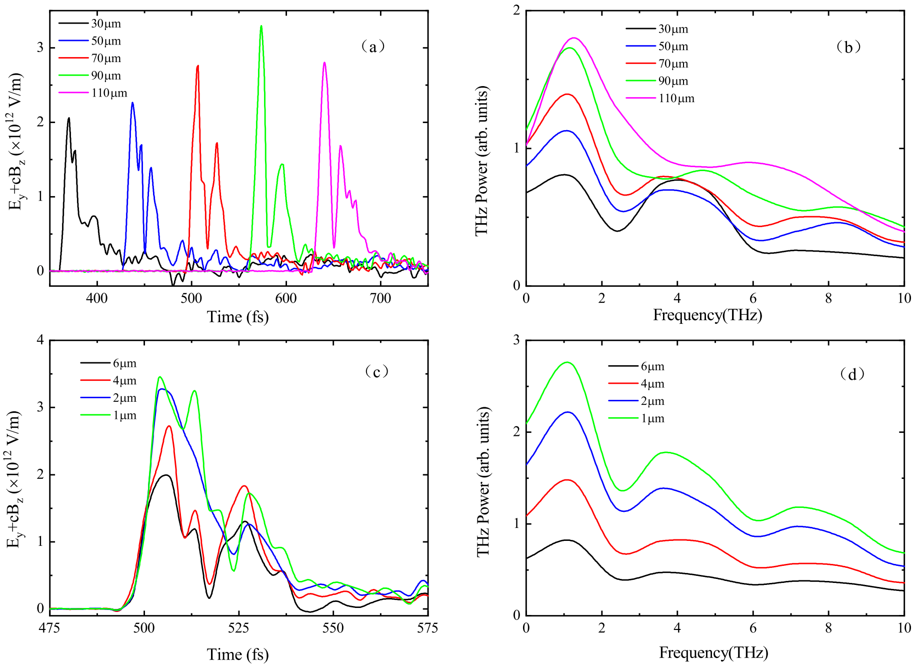

Figure 7. Influence of the target parameters such as length and thickness on THz emission. The dependence of terahertz radiation on different lengths (**a**,**b**) and thicknesses (**c**,**d**) of Target I in the case of TTT. (**a**,**c**) are the time-domain waveforms of the radiated electromagnetic field, and (**b**,**d**) are the corresponding frequency-domain spectrum.

In addition, we performed numerical simulations on the effect of the laser duration on THz emission when keeping the laser input energy constant, as shown in Figure 8. As the laser duration increased, the intensity of the radiated electromagnetic field decreased, and the power of the corresponding THz wave also decreased. The main reason for the above results is that the intensity of the laser decreases with the increase of the laser duration under the condition that the laser input energy remains unchanged. The electron energy is proportional to the intensity of the laser, so this leads to a decrease in the THz wave's intensity when the electron energy decreases. Our results were consistent with the previously reported results, which investigated the effect of laser duration on THz emission [61]. Furthermore, we investigated the effects of SLT and TTT on THz radiation using the controlled variable method under the same conditions for all laser input parameters; so, the effect of changing laser duration on both cases was similar.

Moreover, the laser's pointing stability is a very important parameter, since it may cause the misalignment between the laser focal spot center and the target center. The laser's pointing deviation of less than $0.8r_0$ is currently achievable [44,62,63]. Therefore, we simulated the process of generating THz emission when the laser was $\pm 5\lambda_0$ off the x-axis, as shown in Figure 9. This result indicated that in the case of laser pointing deviation, the radiated electromagnetic field and the corresponding THz emission passing through the detection point would not weaken but increase, and they were much larger than that of the SLT.

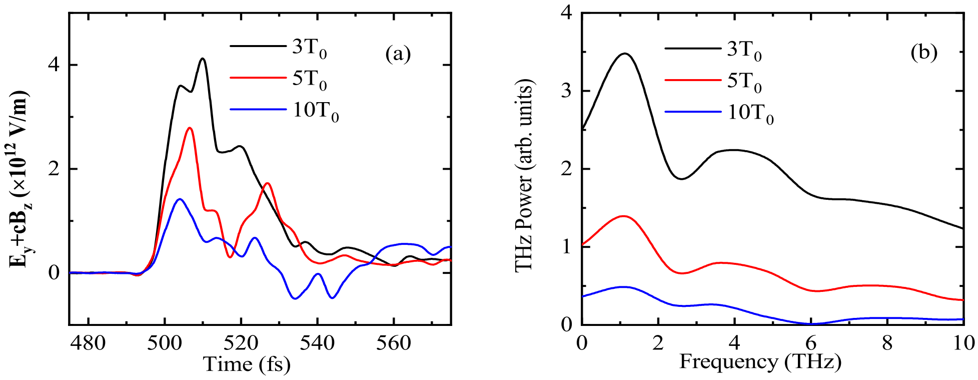

Figure 8. Influence of the different laser durations with $3T_0$, $5T_0$, and $10T_0$ on THz emission for the TTT. (**a**) The time-domain waveforms of the radiated electromagnetic field. (**b**) The frequency-domain spectra.

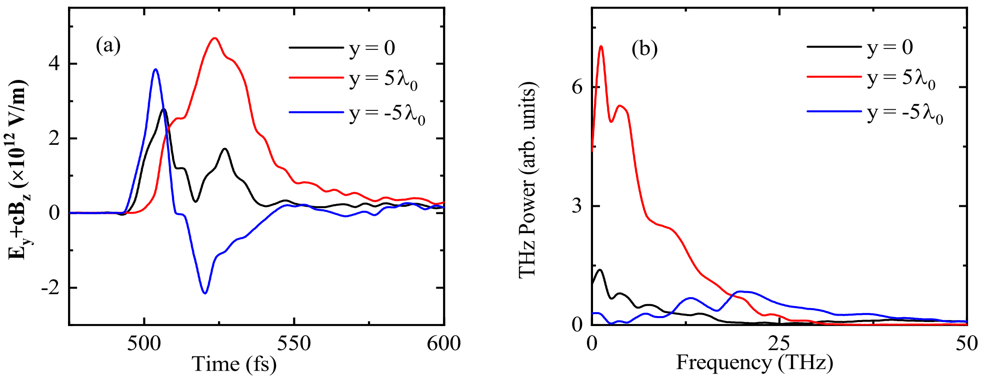

Figure 9. The radiated electromagnetic field passing through the space point $(146.67\lambda_0, -20.0\lambda_0)$ at the (x, y) plane for the different laser pointing deviations. (**a**) The time-domain waveforms of the radiated electromagnetic field. (**b**) The frequency-domain spectra.

6. Conclusions

In summary, we have proposed a novel scheme with an ultra-intense laser pulse irradiating on a T-type target to enhance the THz emission, and the related processes were investigated by using the PIC simulations performance. Compared with the single-layer target, our results show that such a T-type target could not only increase the intensity of terahertz emission by an order of magnitude but also could significantly tune its spatial distribution. The reason for the above results is that the fast electrons controlling the THz emission originate from the longitudinal portion of the T-type target. The direct laser acceleration modulated the electrons very significantly. Finally, the robustness of our scheme was studied with respect to the thickness and length of the longitudinal part. The proposed scheme and simulation results may provide important theoretical and data support for the enhancement of terahertz emission efficiency based on the ultra-intense laser irradiation of solid targets.

Author Contributions: Conceptualization and supervision, C.L. and F.W.; simulations, J.Z., X.B. and C.L.; data analysis, C.L. and F.W.; writing—original draft preparation, J.Z. and X.B.; writing—review and editing, C.L., F.W. and J.Z. All authors have read and agreed to the published version of the manuscript.

Funding: This work was supported by the National Natural Science Foundation of China (NSFC) under Grant Nos. 12005305, 11905169, and the Continue Basic Scientific Research Project under Grant Nos. WDJC-2019-02, and BJ20002501.

Institutional Review Board Statement: Not applicable.

Informed Consent Statement: Not applicable.

Data Availability Statement: The data that support the findings of this study are available from the corresponding author upon reasonable request.

Acknowledgments: The authors would like to thank the anonymous reviewers for their constructive suggestions. Chong Lv would like to thank Zhigang Deng from the Research Center of Laser Fusion, China Academy of Engineering Physics for their fruitful discussions. The PIC simulations were performed on the Tianhe-2 supercomputer (China). The authors are particularly grateful to CFSA at University of Warwick for allowing us to use the EPOCH. The EPOCH code was used under UK EPSRC contract (EP/G055165/1 and EP/G056803/1).

Conflicts of Interest: The authors declare no conflict of interest.

References

1. Hebling, J.; Yeh, K.L.; Hoffmann, M.C.; Nelson, K.A. High-power THz generation, THz nonlinear optics, and THz nonlinear spectroscopy. *IEEE J. Sel. Top. Quantum Electron.* **2008**, *14*, 345–353. [CrossRef]
2. Matsunaga, R.; Shimano, R. Nonequilibrium BCS state dynamics induced by intense terahertz pulses in a superconducting NbN film. *Phys. Rev. Lett.* **2012**, *109*, 187002. [CrossRef] [PubMed]
3. Kampfrath, T.; Tanaka, K.; Nelson, K.A. Resonant and nonresonant control over matter and light by intense terahertz transients. *Nat. Photonics* **2013**, *7*, 680–690. [CrossRef]
4. Globus, T.; Woolard, D.; Khromova, T.; Crowe, T.; Bykhovskaia, M.; Gelmont, B.; Hesler, J.; Samuels, A. THz-spectroscopy of biological molecules. *J. Biol. Phys.* **2003**, *29*, 89–100. [CrossRef]
5. Siegel, P.H. Terahertz technology in biology and medicine. *IEEE Trans. Microw. Theory Tech.* **2004**, *52*, 2438–2447. [CrossRef]
6. Pickwell, E.; Wallace, V. Biomedical applications of terahertz technology. *J. Phys. Appl. Phys.* **2006**, *39*, R301. [CrossRef]
7. Shen, J.L.; Zhang, C. Terahertz nondestructive imaging technology and its application. *Nondestruct. Test.* **2005**, *27*, 146–147.
8. Zheng, X.; Liu, C. Recent development of THz technology and its application in radar and communication system. *J. Microw.* **2010**, *26*, 1–6.
9. Wu, Z.; Fisher, A.S.; Goodfellow, J.; Fuchs, M.; Daranciang, D.; Hogan, M.; Loos, H.; Lindenberg, A. Intense terahertz pulses from SLAC electron beams using coherent transition radiation. *Rev. Sci. Instrum.* **2013**, *84*, 022701. [CrossRef]
10. Hirori, H.; Doi, A.; Blanchard, F.; Tanaka, K. Single-cycle terahertz pulses with amplitudes exceeding 1 MV/cm generated by optical rectification in $LiNbO_3$. *Appl. Phys. Lett.* **2011**, *98*, 091106. [CrossRef]
11. Vicario, C.; Jazbinsek, M.; Ovchinnikov, A.; Chefonov, O.; Ashitkov, S.; Agranat, M.; Hauri, C. High efficiency THz generation in DSTMS, DAST and OH1 pumped by Cr: forsterite laser. *Opt. Express* **2015**, *23*, 4573–4580. [CrossRef]
12. Shalaby, M.; Hauri, C.P. Demonstration of a low-frequency three-dimensional terahertz bullet with extreme brightness. *Nat. Commun.* **2015**, *6*, 5976. [CrossRef] [PubMed]
13. Weling, A.; Hu, B.; Froberg, N.; Auston, D. Generation of tunable narrow-band THz radiation from large aperture photoconducting antennas. *Appl. Phys. Lett.* **1994**, *64*, 137–139. [CrossRef]
14. Cook, D.; Hochstrasser, R. Intense terahertz pulses by four-wave rectification in air. *Opt. Lett.* **2000**, *25*, 1210–1212. [CrossRef] [PubMed]
15. Zhang, L.L.; Wang, W.M.; Wu, T.; Zhang, R.; Zhang, S.J.; Zhang, C.L.; Zhang, Y.; Sheng, Z.M.; Zhang, X.C. Observation of terahertz radiation via the two-color laser scheme with uncommon frequency ratios. *Phys. Rev. Lett.* **2017**, *119*, 235001. [CrossRef]
16. Kim, K.Y.; Taylor, A.; Glownia, J.; Rodriguez, G. Coherent control of terahertz supercontinuum generation in ultrafast laser–gas interactions. *Nat. Photonics* **2008**, *2*, 605–609. [CrossRef]
17. Ma, D.; Dong, L.; Zhang, M.; Wu, T.; Zhao, Y.; Zhang, L.; Zhang, C. Enhancement of terahertz waves from two-color laser-field induced air plasma excited using a third-color femtosecond laser. *Opt. Express* **2020**, *28*, 20598–20608. [CrossRef]
18. Wang, W.M.; Gibbon, P.; Sheng, Z.M.; Li, Y.T. Tunable circularly polarized terahertz radiation from magnetized gas plasma. *Phys. Rev. Lett.* **2015**, *114*, 253901. [CrossRef]
19. Hamster, H.; Sullivan, A.; Gordon, S.; White, W.; Falcone, R. Subpicosecond, electromagnetic pulses from intense laser-plasma interaction. *Phys. Rev. Lett.* **1993**, *71*, 2725. [CrossRef]
20. Hamster, H.; Sullivan, A.; Gordon, S.; Falcone, R. Short-pulse terahertz radiation from high-intensity-laser-produced plasmas. *Phys. Rev. E* **1994**, *49*, 671. [CrossRef]
21. Gopal, A.; Singh, P.; Herzer, S.; Reinhard, A.; Schmidt, A.; Dillner, U.; May, T.; Meyer, H.G.; Ziegler, W.; Paulus, G. Characterization of 700 μJ T rays generated during high-power laser solid interaction. *Opt. Lett.* **2013**, *38*, 4705–4707. [CrossRef] [PubMed]
22. Ding, W.; Sheng, Z.; Koh, W. High-field half-cycle terahertz radiation from relativistic laser interaction with thin solid targets. *Appl. Phys. Lett.* **2013**, *103*, 204107. [CrossRef]
23. Ginzburg, V.; Frank, I. Radiation of a uniformly moving electron due to its transition from one medium into another. *J. Phys. (USSR)* **1945**, *9*, 353–362.
24. Ginsburg, V. Radiation of a uniformly moving electron due to its transition from one medium into another. *Sov. Phys. JETP* **1946**, *16*, 15–28.
25. Liao, G.Q.; Li, Y.T.; Zhang, Y.H.; Liu, H.; Ge, X.L.; Yang, S.; Wei, W.Q.; Yuan, X.H.; Deng, Y.Q.; Zhu, B.J.; et al. Demonstration of coherent terahertz transition radiation from relativistic laser-solid interactions. *Phys. Rev. Lett.* **2016**, *116*, 205003. [CrossRef]

26. Liao, G.; Li, Y.; Liu, H.; Scott, G.G.; Neely, D.; Zhang, Y.; Zhu, B.; Zhang, Z.; Armstrong, C.; Zemaityte, E.; et al. Multimillijoule coherent terahertz bursts from picosecond laser-irradiated metal foils. *Proc. Natl. Acad. Sci. USA* **2019**, *116*, 3994–3999. [CrossRef]
27. Mondal, S.; Wei, Q.; Ding, W.; Hafez, H.A.; Fareed, M.; Laramée, A.; Ropagnol, X.; Zhang, G.; Sun, S.; Sheng, Z.; et al. Aligned copper nanorod arrays for highly efficient generation of intense ultra-broadband THz pulses. *Sci. Rep.* **2017**, *7*, 40058. [CrossRef]
28. Liao, G.Q.; Liu, H.; Scott, G.G.; Zhang, Y.H.; Zhu, B.J.; Zhang, Z.; Li, Y.T.; Armstrong, C.; Zemaityte, E.; Bradford, P.; et al. Towards terawatt-scale spectrally tunable terahertz pulses via relativistic laser-foil interactions. *Phys. Rev. X* **2020**, *10*, 031062. [CrossRef]
29. Potylitsyn, A.P.; Ryazanov, M.I.; Strikhanov, M.N.; Tishchenko, A.A. Radiation from relativistic particles. In *Diffraction Radiation from Relativistic Particles*; Springer: Berlin/Heidelberg, Germany, 2010; pp. 1–28.
30. Yi, L.; Fülöp, T. Coherent diffraction radiation of relativistic terahertz pulses from a laser-driven microplasma waveguide. *Phys. Rev. Lett.* **2019**, *123*, 094801. [CrossRef]
31. Pitarke, J.; Silkin, V.; Chulkov, E.; Echenique, P. Theory of surface plasmons and surface-plasmon polaritons. *Rep. Prog. Phys.* **2006**, *70*, 1. [CrossRef]
32. Riconda, C.; Raynaud, M.; Vialis, T.; Grech, M. Simple scalings for various regimes of electron acceleration in surface plasma waves. *Phys. Plasmas* **2015**, *22*, 073103. [CrossRef]
33. Fedeli, L.; Sgattoni, A.; Cantono, G.; Garzella, D.; Réau, F.; Prencipe, I.; Passoni, M.; Raynaud, M.; Květoň, M.; Proska, J.; et al. Electron acceleration by relativistic surface plasmons in laser-grating interaction. *Phys. Rev. Lett.* **2016**, *116*, 015001. [CrossRef] [PubMed]
34. Macchi, A. Surface plasmons in superintense laser-solid interactions. *Phys. Plasmas* **2018**, *25*, 031906. [CrossRef]
35. Ma, Y.Y.; Sheng, Z.M.; Li, Y.T.; Chang, W.W.; Yuan, X.H.; Chen, M.; Wu, H.C.; Zheng, J.; Zhang, J. Dense quasi-monoenergetic attosecond electron bunches from laser interaction with wire and slice targets. *Phys. Plasmas* **2006**, *13*, 110702. [CrossRef]
36. Nakajima, H.; Tokita, S.; Inoue, S.; Hashida, M.; Sakabe, S. Divergence-free transport of laser-produced fast electrons along a meter-long wire target. *Phys. Rev. Lett.* **2013**, *110*, 155001. [CrossRef]
37. Hu, L.X.; Yu, T.P.; Sheng, Z.M.; Vieira, J.; Zou, D.B.; Yin, Y.; McKenna, P.; Shao, F.Q. Attosecond electron bunches from a nanofiber driven by Laguerre–Gaussian laser pulses. *Sci. Rep.* **2018**, *8*, 7282. [CrossRef]
38. Zeng, Y.; Tian, Y.; Zhou, C.; Li, Z.; Liu, J.; Xu, Z. Experimental study on laser-driven electron collimation along wire targets. *Phys. Plasmas* **2019**, *26*, 012701. [CrossRef]
39. Zeng, Y.; Zhou, C.; Qi, R.; Li, Z.; Sun, H.; Tian, Y.; Liu, J.; Xu, Z. Experimental optimization of the hundred-keV electron source from laser-driven wire target. *Laser Part. Beams* **2020**, *38*, 94–100. [CrossRef]
40. Ong, J.; Ghenuche, P.; Tanaka, K. Electron transport in a nanowire irradiated by an intense laser pulse. *Phys. Rev. Res.* **2021**, *3*, 033262. [CrossRef]
41. Ma, Y.; Sheng, Z.; Gu, Y.; Yu, M.; Yin, Y.; Shao, F.; Yu, T.; Chang, W. High-quality MeV protons from laser interaction with umbrellalike cavity target. *Phys. Plasmas* **2009**, *16*, 034502.
42. Wang, F.; Shen, B.; Zhang, X.; Jin, Z.; Wen, M.; Ji, L.; Wang, W.; Xu, J.; Yu, M.; Cary, J. High-energy monoenergetic proton bunch from laser interaction with a complex target. *Phys. Plasmas* **2009**, *16*, 093112. [CrossRef]
43. Haider, M.M.; Sheng, Z.M. Collimated proton beam from an ultra-intense laser pulse irradiating parallel to the plasma interface. *AIP Adv.* **2021**, *11*, 035221. [CrossRef]
44. Shen, X.; Pukhov, A.; Qiao, B. Monoenergetic High-Energy Ion Source via Femtosecond Laser Interacting with a Microtape. *Phys. Rev. X* **2021**, *11*, 041002. [CrossRef]
45. Li, H.Z.; Yu, T.P.; Hu, L.X.; Yin, Y.; Zou, D.B.; Liu, J.X.; Wang, W.Q.; Hu, S.; Shao, F.Q. Ultra-bright γ-ray flashes and dense attosecond positron bunches from two counter-propagating laser pulses irradiating a micro-wire target. *Opt. Express* **2017**, *25*, 21583–21593. [CrossRef] [PubMed]
46. Wang, W.M.; Sheng, Z.M.; Gibbon, P.; Chen, L.M.; Li, Y.T.; Zhang, J. Collimated ultrabright gamma rays from electron wiggling along a petawatt laser-irradiated wire in the QED regime. *Proc. Natl. Acad. Sci. USA* **2018**, *115*, 9911–9916. [CrossRef] [PubMed]
47. Tokita, S.; Sakabe, S.; Nagashima, T.; Hashida, M.; Inoue, S. Strong sub-terahertz surface waves generated on a metal wire by high-intensity laser pulses. *Sci. Rep.* **2015**, *5*, 8268. [CrossRef] [PubMed]
48. Tian, Y.; Liu, J.; Bai, Y.; Zhou, S.; Sun, H.; Liu, W.; Zhao, J.; Li, R.; Xu, Z. Femtosecond-laser-driven wire-guided helical undulator for intense terahertz radiation. *Nat. Photonics* **2017**, *11*, 242–246. [CrossRef]
49. Teramoto, K.; Tokita, S.; Terao, T.; Inoue, S.; Yasuhara, R.; Nagashima, T.; Kojima, S.; Kawanaka, J.; Mori, K.; Hashida, M.; et al. Half-cycle terahertz surface waves with MV/cm field strengths generated on metal wires. *Appl. Phys. Lett.* **2018**, *113*, 051101. [CrossRef]
50. Zeng, Y.; Zhou, C.; Song, L.; Lu, X.; Li, Z.; Ding, Y.; Bai, Y.; Xu, Y.; Leng, Y.; Tian, Y.; et al. Guiding and emission of milijoule single-cycle THz pulse from laser-driven wire-like targets. *Opt. Express* **2020**, *28*, 15258–15267. [CrossRef]
51. Zhuo, H.; Zhang, S.; Li, X.; Zhou, H.; Li, X.; Zou, D.; Yu, M.; Wu, H.; Sheng, Z.; Zhou, C. Terahertz generation from laser-driven ultrafast current propagation along a wire target. *Phys. Rev. E* **2017**, *95*, 013201. [CrossRef]
52. Arber, T.; Bennett, K.; Brady, C.; Lawrence-Douglas, A.; Ramsay, M.; Sircombe, N.; Gillies, P.; Evans, R.; Schmitz, H.; Bell, A.; et al. Contemporary particle-in-cell approach to laser-plasma modelling. *Plasma Phys. Control. Fusion* **2015**, *57*, 113001. [CrossRef]
53. Ammosov, M.V.; Delone, N.B.; Krainov, V.P. Tunnel ionization of complex atoms and of atomic ions in an alternating electromagnetic field. *Sov. J. Exp. Theor. Phys.* **1986**, *64*, 1191.

54. Shen, X.; Qiao, B.; Zhang, H.; Xie, Y.; Kar, S.; Borghesi, M.; Zepf, M.; Zhou, C.; Zhu, S.; He, X. Electrostatic capacitance-type acceleration of ions with an intense few-cycle laser pulse. *Appl. Phys. Lett.* **2019**, *114*, 144102. [CrossRef]
55. Kemp, A.J.; Sentoku, Y.; Sotnikov, V.; Wilks, S. Collisional relaxation of superthermal electrons generated by relativistic laser pulses in dense plasma. *Phys. Rev. Lett.* **2006**, *97*, 235001. [CrossRef] [PubMed]
56. Luan, S.; Yu, W.; Li, F.; Wu, D.; Sheng, Z.; Yu, M.; Zhang, J. Laser propagation in dense magnetized plasma. *Phys. Rev. E* **2016**, *94*, 053207. [CrossRef]
57. Korneev, P.; d'Humières, E.; Tikhonchuk, V. Gigagauss-scale quasistatic magnetic field generation in a snail-shaped target. *Phys. Rev. E* **2015**, *91*, 043107. [CrossRef]
58. Price, D.; More, R.; Walling, R.; Guethlein, G.; Shepherd, R.; Stewart, R.; White, W. Absorption of ultrashort laser pulses by solid targets heated rapidly to temperatures 1–1000 eV. *Phys. Rev. Lett.* **1995**, *75*, 252. [CrossRef]
59. Raynaud, M.; Kupersztych, J.; Riconda, C.; Adam, J.; Heron, A. Strongly enhanced laser absorption and electron acceleration via resonant excitation of surface plasma waves. *Phys. Plasmas* **2007**, *14*, 092702. [CrossRef]
60. Pukhov, A.; Meyer-ter Vehn, J. Laser wake field acceleration: the highly non-linear broken-wave regime. *Appl. Phys. B* **2002**, *74*, 355–361. [CrossRef]
61. Herzer, S.; Woldegeorgis, A.; Polz, J.; Reinhard, A.; Almassarani, M.; Beleites, B.; Ronneberger, F.; Grosse, R.; Paulus, G.; Hübner, U.; et al. An investigation on THz yield from laser-produced solid density plasmas at relativistic laser intensities. *New J. Phys.* **2018**, *20*, 063019. [CrossRef]
62. Hilz, P.; Ostermayr, T.; Huebl, A.; Bagnoud, V.; Borm, B.; Bussmann, M.; Gallei, M.; Gebhard, J.; Haffa, D.; Hartmann, J.; et al. Isolated proton bunch acceleration by a petawatt laser pulse. *Nat. Commun.* **2018**, *9*, 423. [CrossRef] [PubMed]
63. Danson, C.N.; Haefner, C.; Bromage, J.; Butcher, T.; Chanteloup, J.C.F.; Chowdhury, E.A.; Galvanauskas, A.; Gizzi, L.A.; Hein, J.; Hillier, D.I.; et al. Petawatt and exawatt class lasers worldwide. *High Power Laser Sci. Eng.* **2019**, *7*. [CrossRef]